Comptes rendus - Geoscience 351 (2019) 451–460

Contents lists available at ScienceDirect

Comptes rendus - Geoscience

www.journals.elsevier.com/comptes-rendus-geoscience

Stratigraphy, Sedimentology (Palaeoenvironment)

Holocene palaeogeographical reconstruction and relative sea-level changes in the southeastern part of the island of Samos (Greece)

Niki Evelpidou [a, *], Kosmas Pavlopoulos [b], Konstantinos Vouvalidis [c], George Syrides [c], Maria Triantaphyllou [a], Anna Karkani [a], Theodoros Paraschou [c]

[a] Faculty of Geology & Geoenvironment, National and Kapodistrian University of Athens, Greece
[b] Geography and Planning Department, Paris-Sorbonne University Abu Dhabi, Abu Dhabi, United Arab Emirates
[c] Department of Physical & Environmental Geography, Faculty of Geology, Aristotle University of Thessaloniki, Greece

ARTICLE INFO

Article history:
Received 2 August 2018
Accepted 16 September 2019

Handled by Isabelle Manighetti

Keywords:
Lagoons
Sediment corings
Coastal evolution
East Aegean sea

ABSTRACT

In this paper, we focus on the southeastern coastal zone of the island of Samos (east-central Aegean Sea), in order to reconstruct the evolution of coastal landscapes and the relative sea-level changes during the late Holocene. We use geomorphological mapping, sedimentological and palaeontological proxies of late Holocene coastal deposits from two lagoon environments. We further compare our results with previously published sea-level data and we show that the southeastern part of Samos was characterized by a subsidence trend at least during the late Holocene, with RSL rise rates of ~0.8 mm/yr. Our study additionally highlights that local-scale tectonics is responsible for the evolution of the coastal zone of Samos.

1. Introduction

Samos lies in mid-eastern Aegean Sea at the western edge of a zone of intense earthquakes and seismic faulting (Fig. 1), along the Greater Menderes River (Saroglu et al., 1992; Stiros et al., 2000). Since the 19th century, the island of Samos has been struck by numerous earthquakes of magnitude higher than 6, i.e. at least six earthquakes during the 19th century, of which one in 1904 and one in 1955, with magnitudes of 6.8 and 6.9, respectively (Guidoboni et al., 1994; Papazachos and Papazachou, 1997; Stiros, 1995). Multiple evidence of uplift have been reported in the literature at the northwestern coast of the island (see triangles in Fig. 1) in the form of notches and benches, which might correspond to co-seismic uplifts occurring approximately 500, 1500 and 3600–3900 years ago (Stiros et al., 2000). Conversely, subsidence has been noted on the southeastern coast of the island (see archaeological locations in Fig. 1), as indicated by the presence of submerged ancient remains (e.g., Simosi, 1991; Stiros, 1998; Stiros et al., 2000). However, no geomorphological studies have taken place to better elucidate the late Holocene palaeogeographical evolution of this area.

Palaeoenvironmental and palaeogeographic reconstructions based on a multi-proxy approach are particularly useful in environmental settings where sedimentary processes are strongly affected by different variables such as riverine supply, sea level fluctuations, local and regional tectonics, etc. (Brew et al., 2015; Ghilardi et al., 2014; Girone et al., 2013; Marriner et al., 2014; Vacchi et al., 2017). Such parameters have a primary control on the nature, source and distribution of sediments, and thus on the palaeogeographic evolution of the area. Therefore, different

* Corresponding author.
E-mail address: evelpidou@geol.uoa.gr (N. Evelpidou).

https://doi.org/10.1016/j.crte.2019.09.001
1631-0713/

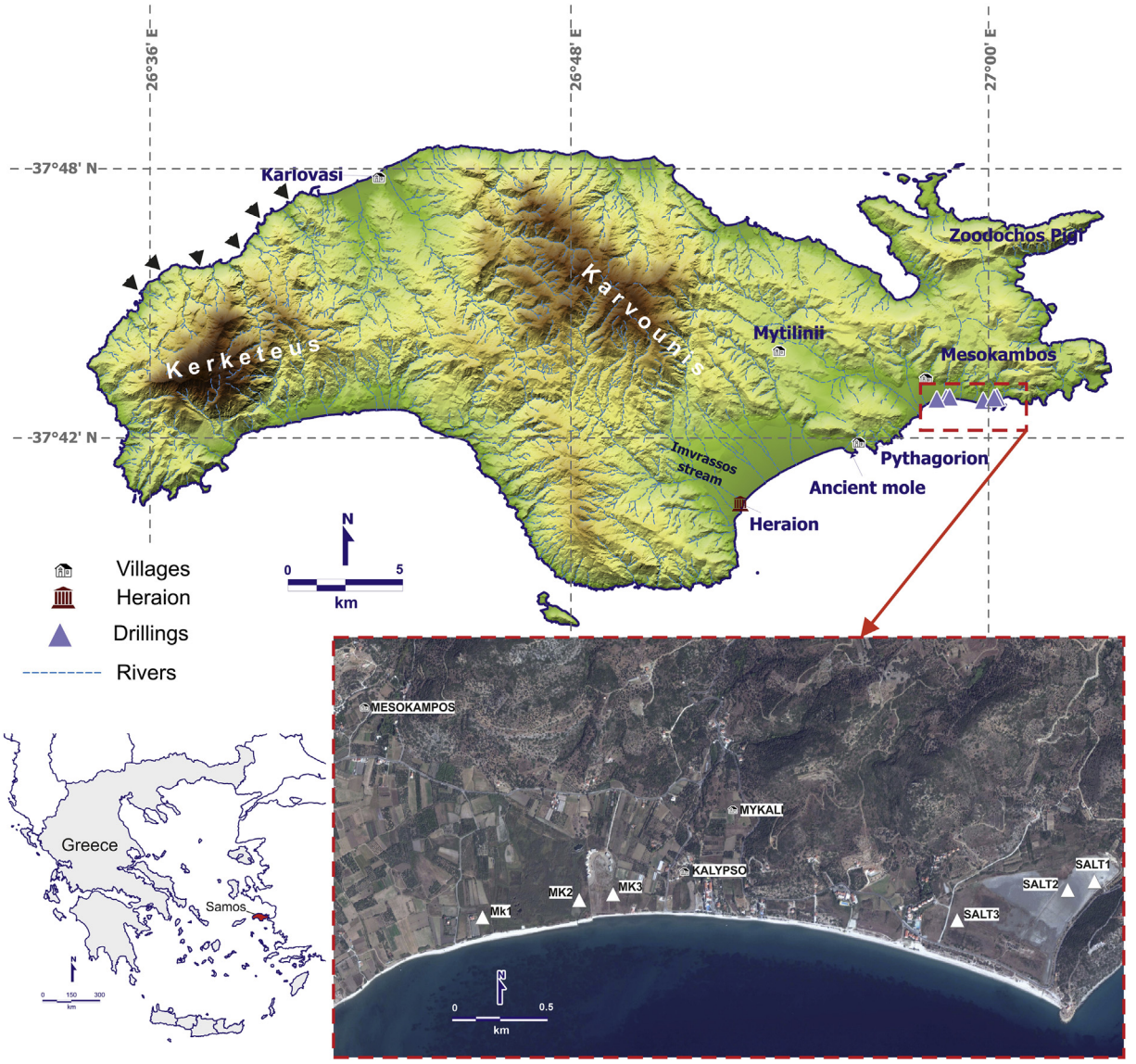

Fig. 1. Study area. In the upper part of the figure (the island of Samos), the black triangles show coastal uplift sites (from Stiros et al., 2000). The bottom right figure shows the location of the boreholes (white triangles).

proxies such as archaeological, sedimentological, biological, etc., are to be utilised in order to gain a wider overview of such processes. Multiproxy investigations are also fundamental to better assess the regional sea-level evolution of the Mediterranean (e.g., Fontana et al., 2017; Melis et al., 2018).

Along the Mediterranean coasts, the sophistication of human constructions has led to a number of archaeological remains, useful in the identification of relative sea-level changes. Since the Mediterranean is characterized by a small tidal range (less than 20 cm in the Aegean Sea (Tsimplis and Blackman, 1997); tide amplitudes of ±0.23 m for the Tyrrhenian Sea and ±0.60 m for the Adriatic Sea (Auriemma and Solinas, 2009), it offers the potential to reconstruct detailed late Holocene sea-level histories.

The study of Holocene shoreline changes and coastal evolution of archaeologically-rich sectors has been the subject of extensive research in the North Aegean (e.g., Ghilardi et al., 2008a, 2008b, 2010, 2012; Kraft et al., 1977; Pavlopoulos et al., 2013; Seeliger et al., 2017; Stock et al., 2016; Syrides et al., 2009; Vacchi et al., 2014; Vouvalidis et al., 2010) and the Cyclades (e.g., Evelpidou et al., 2010, 2012, 2014; Karkani et al., 2018, 2019; Pavlopoulos et al., 2010, 2012).

Palaeoenvironmental reconstructions may significantly improve our understanding of past human–environment interactions and the impact of relative sea-level changes on the coastal environment (e.g., Brückner et al., 2010; Chelli et al., 2017; Fontana et al., 2017; Morhange et al., 2000; Rossi et al., 2015, among many others).

In this context, we investigated the coastal evolution and palaeoshoreline changes of the southeastern part of Samos during the late Holocene using a multiproxy approach with archaeological records, geomorphological, sedimentological, stratigraphical, and palaeontological data. Additionally, this work attempts to provide new RSL (relative sea level) data obtained by sediment cores in order to contribute to a better understanding of RSL evolution in this sector of the Aegean Sea.

2. Regional setting

2.1. Geographical, geological, and geomorphological setting

Samos is located in the mid-eastern Aegean Sea (Fig. 1), at a distance of less than 1.5 km from the West Anatolian coasts. It lies on a shallow plateau extending from the Mt. Samsun Dağı peninsula, to which it was connected during the Pliocene and most of the Pleistocene (Higgins and Higgins, 1996). It is a mountainous island, about 45 km long, covering a surface area of 478 km^2. It is located at the western edge of the tectonically active zone of the Greater Menderes River Graben, in western Turkey (Saroglu et al., 1992).

While the northwestern part of Samos is mountainous with steep cliffs and highly incised streams, the gradient of the topography decreases to the east. In the southeastern part of Samos, in particular, the morphology is characterized by a low, smooth relief with lagoons and extensive sand-gravel beaches developing along the coastal swamps.

According to Chatzipetros et al. (2013), the coastline of Samos is partly controlled by faulting (Fig. 2), with the main coastal and offshore faults forming rather linear coastlines along the same strike. The main geomorphological features are generally aligned in a WNW–ESE direction, coinciding with the main fault zones. The offshore North Samos fault (see Fig. 2) is a long structure of ~25 km, forming a submarine depression at a depth of more than 1000 m (Chatzipetros et al., 2013). This fault demarcates two different geomorphological regions, the island and the deep Samos depression (Fig. 2), reaching depths of more than 1000 m (Chatzipetros et al., 2013).

The main basin of the island (SE), along with smaller valleys and the corresponding drainage system are aligned in a WNW–ESE direction, following the main fault zones. The Pythagorion fault zone is the most predominant structure on the island, controlling the morphology of the area (Fig. 2). The fault is normal, striking WNW–ESE, dipping south at 45°, which manifests in various outcrops where slickenlines are preserved (Chatzipetros et al., 2013).

In the area west of Pythagorion, a rather distinctive tectonic landscape is formed (Fig. 1), where fault scarps clearly delineate two dissimilar areas: the hilly footwall to the north and the flat Pythagorion plain to the south.

2.2. Archaeological setting

The island of Samos is of great archaeological importance; it hosts one of the most important sanctuaries of ancient Greece, Heraion, and the famous aqueduct 'Eupalinous Tunnel'.

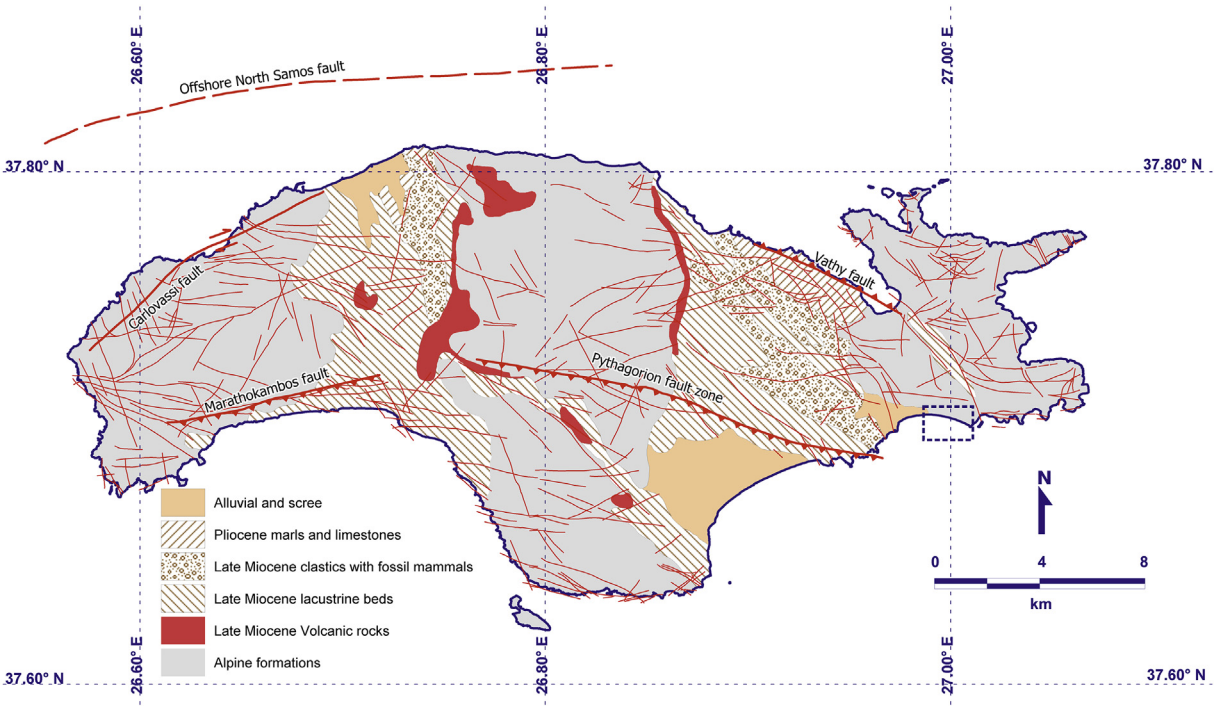

Fig. 2. Lithology along with major and minor faults of the island of Samos (based on Chatzipetros et al. (2013) and Theodoropoulos (1979). The blue dashed rectangle highlights the study area.

The Heraion archaeological site is situated in a swampy plain formed by sediments deposited mostly by Imvrassos stream, at a distance of 7 km from Pythagorion, 100–200 m from the coast, at an elevation of 1–2 m above sea level. A sacred road used to connect Heraion with the ancient town of Samos (modern Pythagorion). Remains of the Road were excavated recently at the archaeological site close to modern Pythagorion.

A submerged ancient mole was constructed in the middle of the 6th century B.C. in order to protect the harbor of Samos from the strong southerly winds (Herodotus III, 60). Ruins of this mole were noted by western travelers in Greece in recent centuries; it has been identified along with a submerged structure clearly seen, parallel to the modern mole, a 19th-century construction. An underwater archaeological survey, however, revealed that the surviving submerged structure corresponds to a mole of the Hellenistic period (300 B.C. or even later). Its base is at depths of 5–10.5 m, while its surviving top is at a depth of 1.8–3.2 m. No clear top, paved surface has been identified offshore, but the surviving top surface is quite regular (Simosi, 1991).

It is important to identify the "functional height" of any archaeological indicator, which is the elevation of specific architectural parts of an archaeological structure in relation to the mean sea level during the period of their use (Morhange and Marriner, 2015). The functional height depends on the structure type, its use and the local tide range. It also defines the minimum elevation of the structure in relation to the local high tides. For example, Antonioli et al. (2007) have stated that the pavements at the top of piers were in the range of 0.5/1.0 m above sea level.

3. Material and methods

The study area is situated in the southeastern part of the island, in the area of Mesokampos (Fig. 1). In order to reconstruct the palaeogeographic evolution of the study area, two sets of boreholes were carried out: one set at Mykali (MK), with three drillings, and one at Psili Ammos (SALT), with three drillings. The boreholes at shallow depths were drilled with a portable vibracoring sampler (Cobra TT) with a diameter of 50 mm. The deepest borehole (MK1') reached 8.93 m in depth, MK2 4.65 m and MK3 4.0 m. SALT1 reached 3.0 m, SALT2 6.0 m, while SALT3 reached 5.0 m in depth (Figs. 3 and 4).

These boreholes provided useful information on depositional phases. The chronostratigraphy of the cores was determined by a series of eight AMS radiocarbon datings on plant, shell, charcoal, and sand with organic material. Radiocarbon dating was carried out at CEntro di DAtazione e Diagnostica (CEDAD), in Lecce, Italy. Radiocarbon ages were calibrated through the online software Calib 7.10 (Stuiver et al., 2017), using the INTCAL13 atmospheric data set for terrestrial samples and the MARINE13 curve for marine samples (Reimer et al., 2013) with a ΔR value of 154 ± 52 estimated for the Aegean Sea (Reimer and McCormac, 2002).

The stratigraphic analysis was accomplished by studying sedimentary sequences through visual inspection of the sediments. The stratigraphy of the late Holocene sediments was studied in detail and analyzed using micropaleontological techniques. Each sample (10 g dry weight) was treated with H_2O_2 to remove the organic matter, washed through 125-μm sieves, and oven-dried at 70 °C. A subset of each sample was obtained using an Otto microsplitter until aliquots of at least 200 benthic foraminifers were collected. Foraminiferal assemblages are expressed in percentages. The microfauna was identified using a Leica APO S8 stereoscope. A scanning electron microscope analyser (SEM Jeol JSM 6360, Department of Historical Geology-Paleontology, Athens, Greece) was used for taxonomical purposes. The taxonomy of the benthic foraminifers identified in this paper is based on Loeblich and Tappan (1988, 1994) and on Bronnimann et al. (1992).

4. Results

4.1. Boreholes lithostratigraphy, faunal evidence and depositional environment

4.1.1. Mykali cores

Based on sedimentological and faunal evidence, two depositional environments were identified, represented by units A_M and B_M (Figs. 3 and 4). In MK1', unit A_M is dominated by clay, with alternations of clayey sand and silty clay. In MK2 and MK3, unit A_M is represented mainly by coarse sand deposits (Fig. 3). Unit A_M is devoid of foraminiferal specimens, except for a few sporadic fragments. Numerous mollusk fragments are present, probably indicating a coastal-river mouth environment. In MK2, the lower part of unit A_M was dated to 477–820 B.C., while in MK2 the middle of unit A_M was dated to 415–778 A.D. (see Table 1).

Unit B_M was only identified in MK1' core. It consists of alternations of clay, silt, clayey silt, and silty clay. The first 50 cm of this unit are barren of foraminiferal content; however, the sporadic presence of charophytes indicates at least a temporary aquatic influence. The interval in-between 50 and 200 cm is characterized by the presence of small-sized *Ammonia* spp. (namely *Ammonia tepida*) and a prominent peak of *Haynesina germanica* (Fig. A.1), indicating a shallow brackish environment, practically a closed lagoon (e.g., Koukousioura et al., 2012).

4.1.2. Psili Ammos cores

Two depositional environments were identified based on sedimentological and faunal evidence, represented by units A_L and B_L (Fig. 4, Figs. A.2, A.3). Unit A_L consists of silty sand, followed by coarse sand and rounded pebbles; it was identified in cores SALT1 and SALT3 (Fig. 4).

Macrofauna remains were noted in SALT3 core with shells such as *Cerastoderma edule, Hydrobia* spp., *Abra spp., Cerithium* spp., *Potamides* spp. Foraminifera in unit A_L were only noted in SALT3, featured by large-sized *Ammonia* spp. (namely *Ammonia beccarii*) and several marine epiphytic foraminiferal indicators such as *Quinqueloculina* spp., *Elphidium* spp., *Neoconorbina* sp., indicating a shallow marine environment with algal vegetation (Fig. A.3).

Unit B_L consists of silty clay, clay and silty sand, and was identified in SALT2 and SALT3. The macrofauna of unit B_L consists of *Abra spp., C. Edule, P.* spp., *H.* spp., *Trochus* spp., *Cyclope* spp., *Bithium* spp. *and C.* spp. In terms of microfauna (Figs. A.2, A.3), the first 320 cm of SALT2 and the first

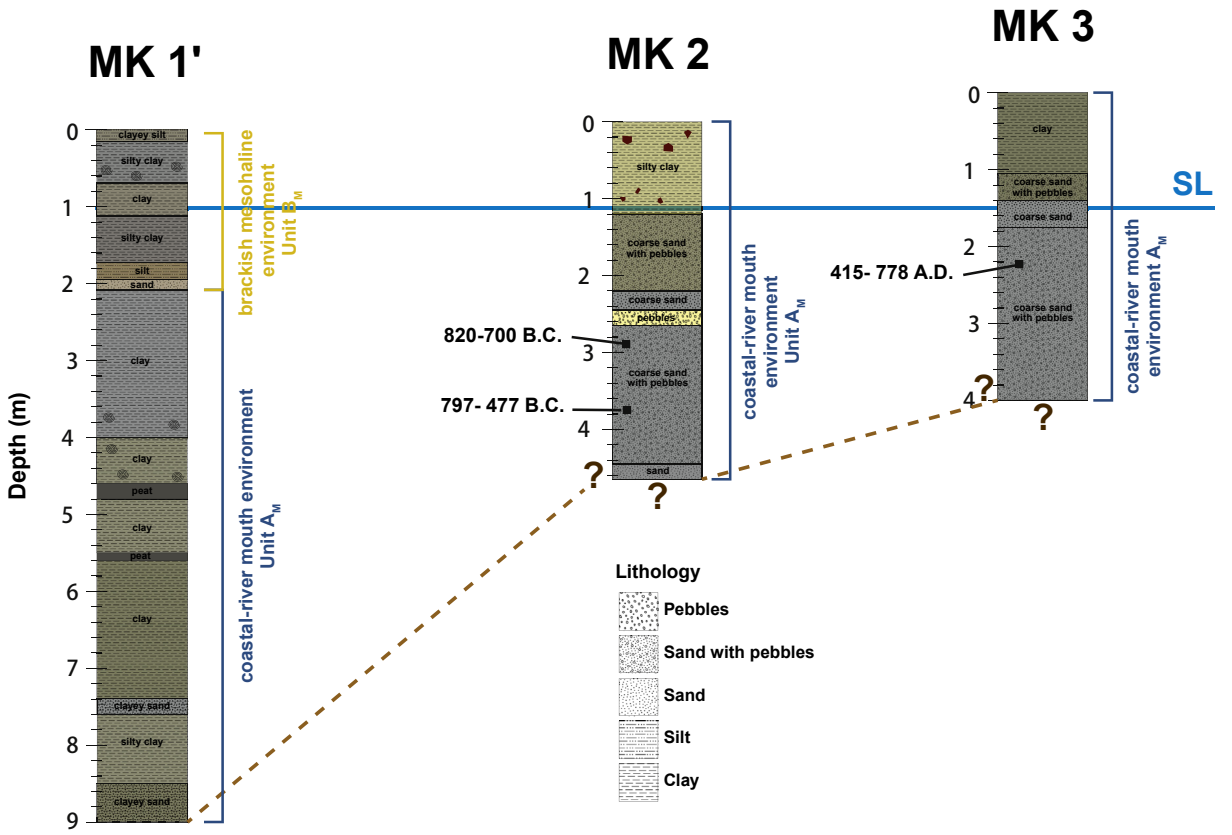

Fig. 3. Stratigraphical columns of MK cores. The brown lines indicate the correlation of environments.

285 cm of SALT3 cores are featured by the intense presence of small-sized *A. tepida* and *H. germanica*, indicating a shallow brackish environment, practically a closed lagoon (Koukousioura et al., 2012). The rest of unit B_L (SALT2, SALT3) displays abundant large-sized *Ammonia* spp. (namely *A. beccarii*), followed by several marine epiphytic foraminiferal indicators such as *Rosalina bradyi*, *Cibicides* spp., *Q.* spp., *Planorbulina mediterranensis*, *E.* spp.,

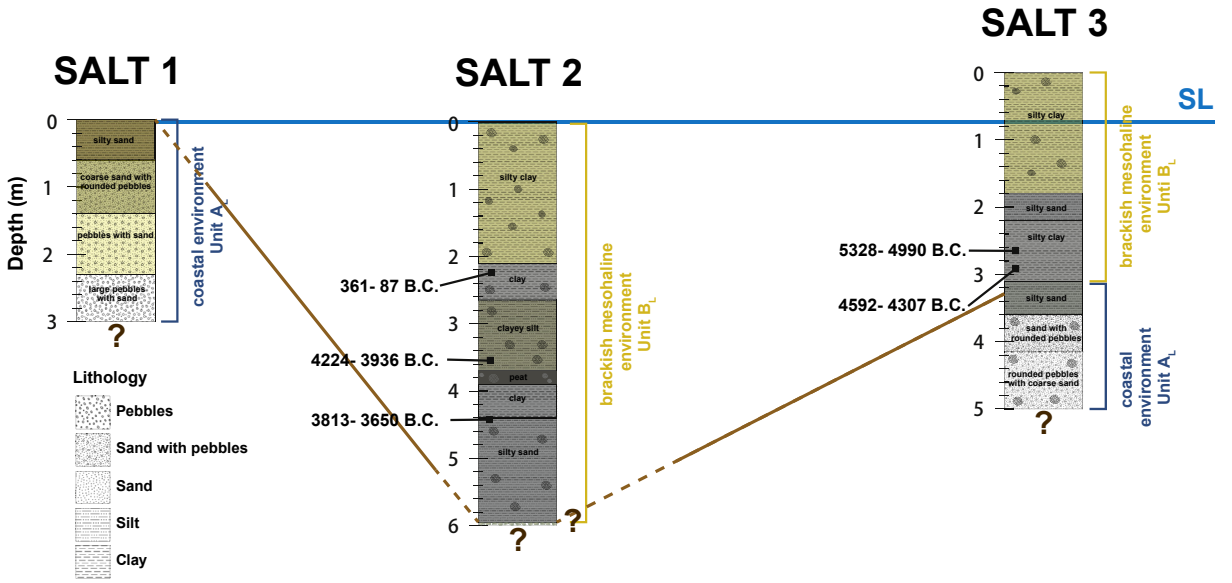

Fig. 4. Stratigraphical columns of SALT cores. The brown lines indicate the correlation of environments.

Table 1
Calibrated radiocarbon ages for dated samples from cores of the Mesokambos area.

No	Sample code	Lab code	Depth below m.s.l. (m)	Material	Conventional R/C age (yr BP)	2σ calibrated age
1.	MK2/2.88	LTL3755A	1.77	Sand with organic material	2566 ± 50	820–700 B.C.
2.	MK2/3.73	LTL3754A	2.62	Charcoal	2508 ± 50	797–477 B.C.
3.	MK3/1.23	LTL3756A	0.72	Plant remains	1411 ± 100	415–778 A.D.
4.	SALT2/2.225	LTL3750A	2.22	Charcoal	2156 ± 50	361–87 B.C.
5.	SALT2/3.53	LTL3749A	3.53	Shell 2 valves cerastoderma	5767 ± 35	4224–3936 B.C.
6.	SALT2/4.41	LTL3748A	4.40	Plant remains	4971 ± 50	3813–3650 B.C.
7.	SALT3/2.65	LTL3751A	1.90	Shell 2 valves	6759 ± 50	5328–4990 B.C.
8.	SALT3/2.92	LTL3752A	2.17	Shell	6121 ± 40	4592–4307 B.C.

Neoconorbina sp., indicating a shallow marine environment with algal vegetation (see electronic supplement). The low abundances of small-sized *Ammonia* spp. suggest brackish influence in an open lagoon (Koukousioura et al., 2012).

Charcoal, shell of *Cerastoderma* with two valves, and plant remains from core SALT2 (unit B_L) found at absolute depths of 2.22 m, 3.53 m, and 4.41 m below mean sea level (msl), were dated to 361- 87 B.C., 4224- 3936 B.C. and 3813-3650 B.C. respectively (Table 1). From core SALT3, the base of unit B_L was dated between 5328 and 4990 B.C. and 4592-4307 B.C., based on a shell with two valves found at an absolute depth of 1.90 m below msl along with a shell found at an absolute depth of 2.17 m msl (Table 1).

5. Discussion

5.1. Relative sea-level changes based on archaeological remains

The archaeological data (see paragraph 2.2) in the southern part of the island of Samos, found below modern sea level, suggest that the area is subsiding (e.g., Stiros, 1998). The submerged Hellenistic mole, parallel to the modern one in the Pythagorion area, lacks a preserved top surface; as a consequence, no precise estimate of relative sea level can be obtained. According to Stiros (1998), a sea-level rise of 2.5 m is likely if one assumes that the original top surface was constructed at least 1 m above the water and corresponds to a surface currently at a depth of 1.5 m. East of the 19th-century fortress, the floor of a 6th-century B.C. sewer is currently a few tens of centimeters below sea level (Stiros, 1998). In order to be functional, its lower level was obviously built above the highest water level in antiquity. It may only testify to a minimum relative sea level rise of 1 m in 1700–2500 years (Stiros, 1998). A prehistoric settlement dated to 2500 B.C., close to the Heraion temple, is currently about 0.4 m above the water (Stiros, 1998). A sea-level rise may be inferred, assuming that this settlement was originally established on a coastal low hill bordered by two branches of the Imbrassos River, flowing in an area free of swamps (Stiros, 1998). The Heraion was always close to the coast (Kyrieleis, 1983), which suggests that the shape of the coast has not changed much since Antiquity. About 1 m of alluvium was deposited on the Sacred Road since its Roman phase, while the surface level of the prehistoric settlement (circa 2000 B.C.) is about 2 m below the ground level of the classical temple (500 B.C.). A number of underground cisterns or wells were constructed in this area, exploiting the surface aquifers of the period; they were at a substantial level beneath the present-day ones, suggesting a RSL rise. The coeval destruction of at least one other temple nearby supports the possibility of a destructive earthquake at circa 530 B.C. (Stiros, 1998).

All the aforementioned archaeological evidence suggests a relative sea-level rise for the study area; however its quantification encompasses many uncertainties. When the structures and their functionality are not directly linked to sea level, they are only indicative of the general direction of sea level. In addition, it is highly likely that antiquities, found today underwater, may have undergone significant erosion, due to storms and wave action (de Graauw, 2014).

5.2. Reconstruction of RSL from sediment corings

We produced a new suite of RSL index points following the protocol developed by Vacchi et al. (2016), which has been used in a number of recent Mediterranean studies (Fontana et al., 2017; Karkani et al., 2017, 2019; Melis et al., 2017, 2018; Vacchi et al., 2018). For samples deposited in a general brackish environment (i.e. LTL3750A, LTL3749A, LTL3748A, LTL3751A, LTL3752A), we considered an indicative range of ±0.5 m (Pavlopoulos et al., 2012; Vacchi et al., 2016). Samples LTL3755A, LTL3754A and LTL3756A were found in a coastal-river mouth environment, representative of the swash zone; therefore, we consider that they were most likely deposited at ±1 m within a former MSL. The vertical error further includes a tidal error of ±0.15 m (HNHS, 2012), a ±0.10 m for the precision of the samples' altitude and an additional ±0.15 m for core stretching/shortening errors (Hijma et al., 2015; Vacchi et al., 2016).

Archaeological remains in our study area consist of coastal and terrestrial structures and difficulties arise in establishing a relationship with a former mean sea level. For this reason, we used the available archaeological data as terrestrial limiting points (see Vacchi et al., 2016). RSL index points should fall below terrestrial limiting points (Vacchi et al., 2016). Most data fit well with the RSL curve of Lambeck and Purcell (2005) and the RSL curve from Poulos et al. (2009) with the notable exception of three shell samples (LTL3751A, LTL3752A, LTL3749A) and the prehistoric settlement (Fig. 5). The age result from sample LTL3749A (at −3.53 m from MSL; 4224–3936 cal yr B.C.) does not appear in stratigraphic order in relation to the other samples of SALT2 borehole. This sample suggests a likely age reversal probably due to a storm event. In a similar manner, samples LTL3751A (at −1.9 m from MSL;

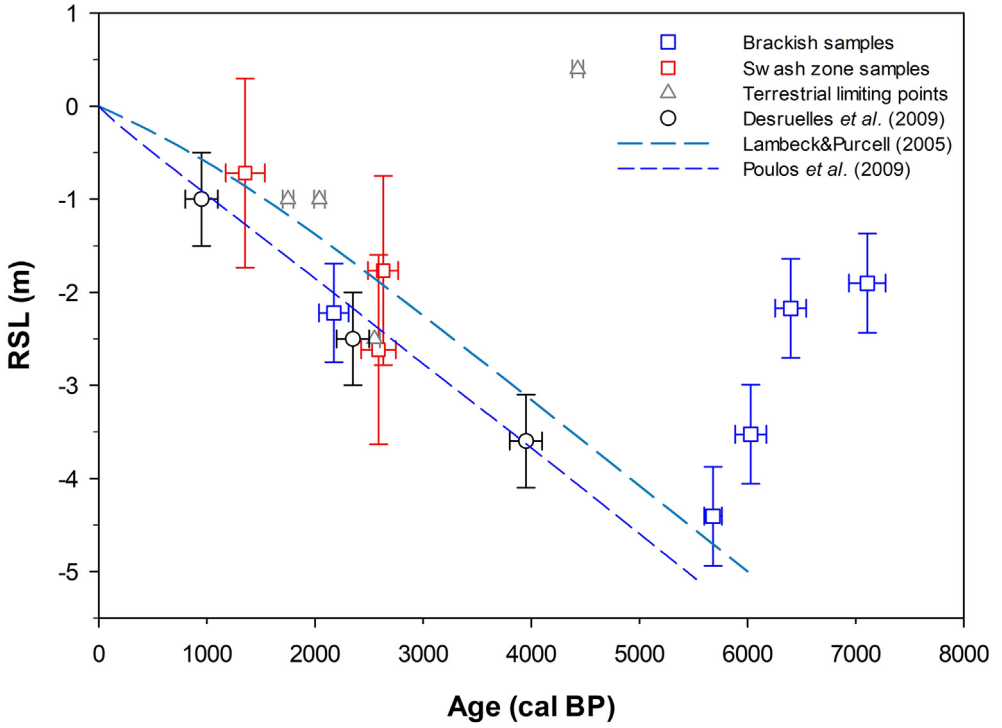

Fig. 5. RSL data produced from this study. The plot shows the samples of this study, in comparison with the RSL reconstruction from Desruelles et al., 2009, Poulos et al. (2009), and the curve predicted by the glacio-hydro-isostatic model (Lambeck and Purcell, 2005). The archaeological data (i.e. ancient mole, cemetery, ancient sewer and prehistoric settlement) were used as terrestrial limiting points.

5328–4990 cal yr B.C.) and LTL3752A (−2.17 from SL; 4592–4307 cal yr B.C.) provide an older age in relation to the neighboring boreholes. Although we may consider that the adjacent borehole data could be underestimated, most likely the aforementioned samples are outliers, considering that they appear overestimated in relation to all other dated samples. The apparently older dates, from core SALT3, could also be due to manmade activities, as the lagoon had been used for salt production activities until relatively recently.

It seems that the area of Mykali from at least 797–477 cal yr B.C. used to be a coastal-river mouth environment, as indicated by the numerous mollusk fragments. It should be noted that Unit A_M in core MK1′ is composed of finer sediments in relation to MK2 and MK3 (coarser), which could be owed to the location of the cores, in relation to the river network. MK2 and MK3 are located close to a first-order stream, providing material from directly upstream. MK1' on the other hand could have been supplied by the two third- and second-order streams, located on its western part, by the longshore current, which has a general direction from west to east. The area of Mykali progressively turned into a shallow brackish environment, practically a closed lagoon, which gradually dried; however, it was aquatically influenced at least temporarily. The schema of Fig. A4a depicts the palaeogeographical evolution of the Mykali area.

The area at Psili Ammos used to be a closed lagoon from about 4224 to 3936 cal yr B.C. Before that and until at least 4592–4307 cal yr B.C., the area used to be a shallow marine environment with algal vegetation, and in fact the low abundances of small-sized *Ammonia spp.* indicate brackish influence in an open lagoon. The Psili Ammos existing configuration appears to have recorded the continuous shoreline transgression and the relocation of the sandy spit towards the SW to its present location. The schema of Fig. A4b depicts the palaeogeographical evolution of the Psili Ammos area.

The ^{14}C dating from organic material and shells was used to reconstruct the relative sea-level changes of Samos utilizing complementary archaeological data (Fig. 5). In order to better assess the results obtained, we compared our data with RSL reconstructions from the Cyclades (Desruelles et al., 2009; Poulos et al., 2009), an area characterized by relatively low seismicity and the absence of large earthquakes (Sakellariou and Galanidou, 2015; Vamvakaris et al., 2016). According to Desruelles et al., 2009, RSL in the northern Cyclades (Mykonos, Delos and Rhenia Islands) was at −3.6 ± 0.5 m at ~ 2000 B.C., at −2.5 ± 0.5 m at ~400 B.C., and at −1.0 ± 0.5 m at ~1000 A.D. (Fig. 5). We further plotted the RSL curve produced by Poulos et al. (2009) for the Cycladic area (central Aegean Sea). Based on our findings, an average rate of RSL rise of 0.8 ± 0.2 mm/yr may be estimated since ~5700 years cal BP. For comparison, the average rate of RSL rise in the northern Cyclades, based on the findings of Desruelles et al., 2009, may be estimated at ~1 mm/yr, while Poulos et al. (2009) have estimated a RSL rise of 0.9 mm/yr for the last 5000

years in the Cyclades. Although the resolution of our data does not allow us to discriminate small differences, it seems likely that the RSL rise trend in our study area is smaller compared to the Cyclades.

5.3. Neotectonic implications

The compilation of our RSL data in comparison with previously available data in the central Aegean (Cyclades) suggests that the southeastern part of Samos is characterized by a RSL rise. There is a general agreement between our results and the published RSL reconstructions from the Cyclades, and similarities are observed in the late Holocene RSL evolution. A tectonic subsidence trend in the Cyclades has been noted by various authors (e.g., Desruelles et al., 2009; Evelpidou et al., 2012; Karkani et al., 2017, 2019; Sakellariou and Galanidou, 2015). Comparable rates of RSL rise are found in our study, when comparing our data with those of the Cyclades.

The two most significant features in the study area are the two main active normal faults: the Pythagorion fault zone and the Vathy fault (see Fig. 2), striking WNW–ESE (Chatzipetros et al., 2013). In fact, the corings are located relatively near the footwall of the Pythagorion fault, which is the most prominent structure of the island of Samos dominating the morphology in this sector of the island (Chatzipetros et al., 2013). According to Pavlides et al. (2009), the Pythagorion fault has an earthquake potential magnitude in the order of 6.6.

However, according to the results of our study, the study area is characterized by a RSL rise trend, at least during the Holocene. This may suggest that the expected vertical displacements related with the major faults of the area were canceled out by other faults dipping in the opposite direction, as some of those indicated in Fig. 2. Stiros et al. (2000) has reported earthquakes being responsible for coastal uplift in the NW of Samos, which would have been extremely strong, especially close to the raised shorelines (northwestern Samos). According to Pavlides et al. (2009), the Karlovassi fault on the NW coast of Samos has an earthquake potential magnitude of 6.5, while Chatzipetros et al. (2013) note a maximum magnitude of 6.4. The raised shorelines were assigned to three earthquakes that occurred approximately 500, possibly 1500 and 3600–3900 years ago (Stiros et al., 2000). Such an earthquake may have been the cause for the offset of the drums of the Heraion (6th c. B.C.) monumental temple in Samos (Stiros, 1996; Stiros et al., 2000). At the nearby island of Ikaria, an unregistered earthquake after 950–1150 A.D. uplifted the NE coast of the island by about 1 m (Stiros et al., 2011). According to Stiros et al. (2000), the topography and bathymetry gradients of the NW part of Samos and of the NE part of the adjacent Ikaria Island seem to be controlled by a major normal fault or a normal fault zone. The uplifted shorelines at Samos are, however, confined to a geographically limited area, about 10 km wide.

Based on the evidence presented above, it becomes clear that local-scale tectonics is responsible for the evolution of the coastal zone of Samos. The present stress regime, which began in the Pliocene–Quaternary, is related to the NNE–SSW trending extension of the Aegean Sea (Chatzipetros et al., 2013; Mountrakis et al., 2003).

6. Conclusions

The palaeogeographic reconstruction of the southeastern part of the island of Samos provided new insights on the coastal evolution of the study area as well as on the RSL evolution in the mid-eastern Aegean Sea during the late Holocene. Previously published archaeological data from the study area suggested a subsidence regime. Our study has shown that the southeastern part of Samos is indeed under a RSL rise trend, at an average rate of ~0.8 ± 0.2 mm/yr since ~5700 cal BP, as suggested by the comparison of our results with previously published sea-level data. Taking into account that evidence of uplift has been reported on the northwestern part of the island, it appears that local-scale tectonics has shaped the present-day coastal zone of the island.

Acknowledgments

Authors would like to thank Mr. Mouzos Vassilis for his help on all topographical issues. We also thank an anonymous reviewer and the associate editor Isabelle Manighetti, whose constructive comments and suggestions improved an earlier version of this paper.

Appendix A. Supplementary data

Supplementary data to this article can be found online at https://doi.org/10.1016/j.crte.2019.09.001.

References

Antonioli, F., Anzidei, M., Lambeck, K., Auriemma, R., Gaddi, D., Furlani, S., Orrù, P., Solinas, E., Gaspari, A., Karinja, S., Kovačić, V., Surace, L., 2007. Sea-level change during the Holocene in Sardinia and in the northeastern Adriatic (central Mediterranean Sea) from archaeological and geomorphological data. Quat. Sci. Rev. 26 (19–21), 2463–2486. https://doi.org/10.1016/j.quascirev.2007.06.022.

Auriemma, R., Solinas, E., 2009. Archaeological remains as sea level change markers: a review. Quat. Int. 206, 134–146.

Brew, D.S., Horton, B.P., Evans, G., Innes, J.B., Shennan, I., 2015. Holocene sea-level history and coastal evolution of the north-western Fenland, eastern England. Proc. Geol. Assoc. 126 (1), 72–85. https://doi.org/10.1016/j.pgeola.2014.12.001.

Bronnimann, P., Whittaker, J.E., Zaninetti, L., 1992. Brackish water foraminifers from mangrove sediments of southwestern Viti Levu, Fiji islands, southwest Pacific. Rev. Paleobiol. 11 (1), 13–65.

Brückner, H., Kelterbaum, D., Marunchak, O., Porotov, A., Vött, A., 2010. The Holocene sea level story since 7500 BP - lessons from the eastern mediterranean, the Black and the Azov Seas. Quat. Int. 225 (2), 160–179.

Chatzipetros, A., Kiratzi, A., Sboras, S., Zouros, N., Pavlides, S., 2013. Active faulting in the north-eastern Aegean Sea islands. Tectonophysics 597–598, 106–122.

Chelli, A., Pappalardo, M., Bini, M., Brückner, H., Neri, G., Neri, M., Spada, G., 2017. Assessing tectonic subsidence from estimates of Holocene relative sea-level change: an example from the NW Mediterranean (Magra Plain, Italy). Holocene 27 (12), 1988–1999. https://doi.org/10.1177/0959683617715688.

de Graauw, A., 2014. The Long-Term Failure of Rubble Mound Breakwaters. Méditerranée [Online], Varia. https://mediterranee.revues.org/7078.

Desruelles, S., Fouache, É., Ciner, A., Dalongeville, R., Pavlopoulos, K., Kosun, E., Coquinot, Y., Potdevin, J.-L., 2009. Beachrocks and sea-level changes since middle Holocene: comparison between the insular group of Mykonos–Delos–Rhenia (Cyclades, Greece) and the

southern coast of Turkey. Glob. Planet. Chang. 66, 19–33. https://doi.org/10.1016/j.gloplacha.2008.07.009.
Evelpidou, N., Pavlopoulos, K., Vassilopoulos, A., Triantaphyllou, M., Vouvalidis, K., Syrides, G., 2010. Yria (western Naxos island, Greece): sea-level changes in upper Holocene and palaeogeographical reconstruction. Geodin. Acta 23, 233–240.
Evelpidou, N., Pavlopoulos, K., Vassilopoulos, A., Triantaphyllou, M., Vouvalidis, K., Syrides, G., 2012. Holocene palaeogeographical reconstruction of the western part of Naxos island (Greece). Quat. Int. 266, 81–93. https://doi.org/10.1016/j.quaint.2011.08.002.
Evelpidou, N., Melini, D., Pirazzoli, P., Vassilopoulos, A., 2014. Evidence of repeated late Holocene rapid subsidence in the SE Cyclades (Greece) deduced from submerged notches. Int. J. Earth Sci. 103 (1), 381–395. https://doi.org/10.1007/s00531-013-0942-0.
Fontana, A., Vinci, G., Tasca, G., Mozzi, P., Vacchi, M., Bivi, G., Salvador, S., Rossato, S., Antonioli, F., Asioli, A., Bresolin, M., Di Mario, F., Hajdas, I., 2017. Lagoonal settlements and relative sea level during Bronze Age in northern Adriatic: geoarchaeological evidence and paleogeographic constraints. Quat. Int. 439, 17–36. https://doi.org/10.1016/j.quaint.2016.12.038.
Ghilardi, M., Kunesch, S., Styllas, M., Fouache, E., 2008a. Reconstruction of Mid-Holocene sedimentary environments in the central part of the Thessaloniki Plain (Greece), based on microfaunal identification, magnetic susceptibility and grain-size analyses. Geomorphology 97, 617–630.
Ghilardi, M., Fouache, E., Queyrel, F., Syrides, G., Vouvalidis, K., Kunesch, S., Styllas, M., Stiros, S., 2008b. Human occupation and geomorphological evolution of the thessaloniki plain (Greece) since mid Holocene. J. Archaeol. Sci. 35, 111–125.
Ghilardi, M., Genç, A., Syrides, G., Bloemendal, J., Psomiadis, D., Paraschou, T., Kunesch, S., Fouache, E., 2010. Reconstruction of the landscape history around the remnant arch of the klidhi roman bridge, Thessaloniki plain, north central Greece. J. Archaeol. Sci. 37, 178–191.
Ghilardi, M., Psomiadis, D., Cordier, S., Delanghe-Sabatier, D., Demory, F., Hamidi, F., Paraschou, T., Dotsika, E., Fouache, E., 2012. The impact of rapid early- to mid- Holocene palaeoenvironmental changes on Neolithic settlement at Nea Nikomideia, Thessaloniki Plain, Greece. Quat. Int. 266, 47–61.
Ghilardi, M., Psomiadis, D., Pavlopoulos, K., Çelka, S.M., Fachard, S., Theurillat, T., Verdan, S., Knodell, A.R., Theodoropoulou, T., Bicket, A., Bonneau, A., Delanghe-Sabatier, D., 2014. Mid- to late Holocene shoreline reconstruction and human occupation in ancient Eretria (south central euboea, Greece). Geomorphology 208, 225–237. https://doi.org/10.1016/j.geomorph.2013.12.006.
Girone, A., Capotondi, L., Ciaranfi, N., Di Leo, P., Lirer, F., Maiorano, P., Marino, M., Pelosi, N., Pulice, I., 2013. Paleoenvironmental changes at the lower Pleistocene Montalbano Jonico section (southern Italy): global versus regional signals. Palaeogeogr. Palaeoclimatol. Palaeoecol. 371, 62–79.
Guidoboni, E., Comastri, A., Traina, G., Rom Istituto Nazionale di Geofisica, 1994. Catalogue of Ancient Earthquakes in the Mediterranean Area up to the 10th Century. Istituto nazionale di geofisica, Rome, p. 504.
Herodotus, 440 B.C.E, the History of Herodotus, Translated by George Rawlinson, Book III.
Hijma, M., Engelhart, S.E., Tornqvist, T.E., Horton, B.P., Hu, P., Hill, D., 2015. A protocol for a geological sea-level database. In: Shennan, I., Long, A., Horton, B.P. (Eds.), Handbook of Sea Level Research. Wiley, pp. 536–553.
Higgins, D.M., Higgins, R., 1996. A Geological Companion to Greece and the Aegean. Duckworth, Great Britain.
HNHS (Hellenic Navy Hydrographic Service), 2012. Statistical Data of Sea Level from Greek Harbors. HNHS, Athens (in Greek).
Karkani, A., Evelpidou, N., Vacchi, M., Morhange, C., Tsukamoto, S., Frechen, M., Maroukian, H., 2017. Tracking shoreline evolution in central Cyclades (Greece) using beachrocks. Mar. Geol. 388, 25–37. https://doi.org/10.1016/j.margeo.2017.04.009.
Karkani, A., Evelpidou, N., Giaime, M., Marriner, N., Maroukian, H., Morhange, C., 2018. Late Holocene palaeogeographical evolution of Paroikia Bay (Paros Island, Greece). C. R. Geoscience 350 (5), 202–211. https://doi.org/10.1016/j.crte.2018.04.004.
Karkani, A., Evelpidou, N., Giaime, M., Marriner, N., Morhange, C., Spada, G., 2019. Late Holocene sea-level evolution of Paros Island (Cyclades, Greece). Quat. Int. 500, 139–146. https://doi.org/10.1016/j.quaint.2019.02.027.
Koukousioura, O., Triantaphyllou, M.V., Dimiza, M.D., Pavlopoulos, K., Syrides, G., Vouvalidis, K., 2012. Benthic foraminiferal evidence and paleoenvironmental evolution of Holocene coastal plains in the Aegean Sea (Greece). Quat. Int. 261, 105–117.
Kraft, J.-C., Aschenbrenner, S.-E., Rapp, G., 1977. Palaeogeographic reconstructions of Coastal Aegean archaeological sites. Science 195, 941–947.
Kyrieleis, H., 1983. The Heraion at Samos. Krini, Athens.
Lambeck, K., Purcell, A., 2005. Sea-level change in the Mediterranean Sea since the LGM: model predictions for tectonically stable areas. Quat. Sci. Rev. 24, 1969–1988.
Loeblich, A.R., Tappan, H., 1988. Foraminiferal Genera and Their Classification. Van Nostrand Reinhold, New York, 545 p.
Loeblich, A.R., Tappan, H., 1994. Foraminifera of the Sahul Self and Timor Sea. Cushman Foundation for Foraminiferal Research Special Publication 31, Washington, 661 p.
Marriner, N., Morhange, C., Faivre, S., Flaux, C., Vacchi, M., Miko, S., Dumas, V., Boetto, G., Radic Rossi, I., 2014. Post-Roman sea-level changes on Pag Island (Adriatic Sea): dating Croatia's “enigmatic” coastal notch? Geomorphology 221, 83–94. https://doi.org/10.1016/j.geomorph.2014.06.002.
Melis, R.T., Depalmas, A., Di Rita, F., Montis, F., Vacchi, M., 2017. Mid to late Holocene environmental changes along the coast of western Sardinia (Mediterranean Sea). Glob. Planet. Chang. 155, 29–41. https://doi.org/10.1016/J.GLOPLACHA.2017.06.001.
Melis, R.T., Di Rita, F., French, C., Marriner, N., Montis, F., Serreli, G., Sulas, F., Vacchi, M., 2018. 8000 years of coastal changes on a western Mediterranean island: a multiproxy approach from the Posada plain of Sardinia. Mar. Geol. 403, 93–108. https://doi.org/10.1016/j.margeo.2018.05.004.
Morhange, C., Goiran, J.P., Bourcier, M., Carbonel, P., Le Campion, J., Rouchy, J.M., Yon, M., 2000. Recent Holocene paleo-environmental evolution and coastline changes of kition, larnaca, Cyprus, mediterranean sea. Mar. Geol. 170 (1–2), 205–230. https://doi.org/10.1016/S0025-3227(00)00075-X.
Morhange, C., Marriner, N., 2015. Archeological and biological relative sea-level indicators. In: Shennan, I., Long, A.J., Horton, B.P. (Eds.), Handbook of Sea-Level Research. John Wiley & Sons, Chichester, UK, pp. 146–156.
Mountrakis, D., Kilias, A., Vavliakis, E., Psilovikos, A., Thomaidou, E., 2003. Neotectonic map of Samos island (Aegean Sea, Greece): implication of geographical information systems in the geological mapping. In: Proc. 4th European Congress on Regional Geoscientific Cartography and Information Systems, Bologna, Italy, pp. 11–13.
Papazachos, B., Papazachou, C., 1997. The Earthquakes of Greece. Ziti, Thessaloniki (in Greek).
Pavlides, S., Tsapanos, T., Zouros, N., Sboras, S., Koravos, G., Chatzipetros, A., 2009. Using active fault data for assessing seismic hazard: a case study from Ne Aegean Sea, Greece. In: Proc. XVII International Conference on Soil Mechanics & Geotechnical Engineering, 2-3 October 2009, Alexandria, Egypt, pp. 1–14.
Pavlopoulos, K., Triantaphyllou, M.V., Karkanas, P., Kouli, K., Syrides, G., Vouvalidis, K., Palyvos, N., Tsourou, T., 2010. Paleoenvironmental evolution and prehistoric human environment, in the embayment of Palamari (Skyros Island, Greece) during middlelate Holocene. Quat. Int. 216, 41–53.
Pavlopoulos, K., Kapsimalis, V., Theodorakopoulou, K., Panagiotopoulos, I., 2012. Vertical displacement trends in the Aegean coastal zone (NE Mediterranean) during the Holocene assessed by geo-archaeological data. Holocene 22 (6), 717–728. https://doi.org/10.1177/0959683611423683.
Pavlopoulos, K., Fouache, E., Sidiropoulou, M., Triantaphyllou, M., Vouvalidis, K., Syrides, G., Gonnet, A., Greco, E., 2013. Palaeoenvironmental evolution and sea-level changes in the coastal area of NE Lemnos Island (Greece) during the Holocene. Quat. Int. 308–309, 80–88. https://doi.org/10.1016/j.quaint.2012.06.024.
Poulos, S.E., Ghionis, G., Maroukian, H., 2009. Sea-level rise trends in the Attico–Cycladic region (Aegean Sea) during the last 5000 years. Geomorphology 107, 10–17. https://doi.org/10.1016/j.geomorph.2007.05.022.
Reimer, P.J., McCormac, F.G., 2002. Marine radiocarbon reservoir correction for the Mediterranean and Aegean Seas. Radiocarbon 44 (1), 159–166. https://doi.org/10.1017/S0033822200064766.
Reimer, P.J., Edouard Bard, B., Alex Bayliss, B., Warren Beck, B.J., Paul Blackwell, B.G., Christopher Bronk Ramsey, B., 2013. Intcal13 and Marine13 radiocarbon age calibration curves 0–50,000 Years cal bp. Radiocarbon 55, 1869–1887. https://doi.org/10.1017/S0033822200048864.
Rossi, V., Sammartino, I., Amorosi, A., Sarti, G., De Luca, S., Lena, A., Morhange, C., 2015. New insights into the palaeoenvironmental evolution of Magdala ancient harbour (Sea of Galilee, Israel) from ostracod assemblages, geochemistry and sedimentology. J. Archaeol. Sci. 54, 356–373. https://doi.org/10.1016/j.jas.2014.05.010.

Sakellariou, D., Galanidou, N., 2015. Pleistocene submerged landscapes and Palaeolithic archaeology in the tectonically active Aegean region. Geol. Soc. London Spec. Publ. 411, 145–178. https://doi.org/10.1144/SP411.9.

Saroglu, F., Emre, O., Kuscu, I., 1992. Active Fault Map of Turkey, 1: 1,000,000 Scale. General Directorate of Mineral Research and Exploration(MTA), Ankara.

Seeliger, M., Pint, A., Frenzel, P., Feuser, S., Pirson, F., Riedesel, S., Brückner, H., 2017. Foraminifera as markers of Holocene sea-level fluctuations and water depths of ancient harbours—a case study from the Bay of Elaia (W Turkey). Palaeogeogr. Palaeoclimatol. Palaeoecol. 482, 17–29.

Simosi, A., 1991. Underwater excavation research in the ancient harbour of Samos: september-October 1988. Int. J. Naut. Archaeol. 20, 281–298.

Stiros, S., 1995. Archaeological evidence of antiseismic constructions in antiquity. An. Geofis. 38, 725–736.

Stiros, S., 1996. Identification of earthquakes from archaeological data: criteria, limitations and pitfalls. In: Stiros, S., Jones, R. (Eds.), Archaeoseismology. Fitch Laboratory, Oxford, pp. 129–152 (occasional. paper 7).

Stiros, S., 1998. Late Quaternary coastal changes in Samos island, Greece – morphotectonics, paleoseismology, archaeology. Guidebook for the Samos Island Fieldtrip UNESCO IGCP 367, INQUA Shorelines and Neotectonics Commissions Conference, Joint Meeting on Rapid Coastal Changes in the Late Quaternary: Processes, Causes, Modeling, Impacts on Coastal Zones, Greece, 10-19 September 1998. Municipality of Pythagorion, Samos, p. 49.

Stiros, S.C., Laborel, J., Laborel-Deguen, F., Papageorgiou, S., Evin, J., Pirazzoli, P.A., 2000. Seismic coastal uplift in a region of subsidence: Holocene raised shorelines of Samos island, Aegean Sea, Greece. Mar. Geol. 170, 41–58.

Stiros, S.C., Laborel, J., Laborel-Deguen, F., Morhange, C., 2011. Quaternary and Holocene coastal uplift in Ikaria island, Aegean Sea. Geodin. Acta 24 (3–4), 123–131.

Stock, F., Stock, F., Knipping, M., Pint, A., Ladstätter, S., Delile, H., Heiss, A.G., Laermanns, H., Mitchell, P.D., Ployer, R., Steskal, M., Thanheiser, U., 2016. Human impact on Holocene sediment dynamics in the eastern Mediterranean – the example of the roman harbour of ephesus. Earth Surf. Process. Landforms 41, 980–996.

Stuiver, M., Reimer, P.J., Reimer, R.W., 2017. CALIB 7.1 [WWW program] at. accessed 2017-4-10. http://calib.org.

Syrides, G., Albanakis, K., Vouvalidis, K., Pilali, A., Papasteriou, A., Papaefthimiou- Papanthimou, A., Ghilardi, M., Fouache, E., Paraschou, T., Psomiadis, D., 2009. Holocene palaeogeography of the northern margins of Giannitsa plain in relation to the prehistoric site of Archontiko (macedoniae Greece). Z. Geomorphol. 53, 71–82.

Theodoropoulos, D., 1979. Geological Map of Greece, 1:50,000 Scale. Neon Karlovasi and Limin Vatheos Sheets. IGME, Athens.

Tsimplis, M.N., Blackman, D., 1997. Extreme sea-level distribution and return periods in the Aegean and Ionian Seas. Estuar. Coast Shelf Sci. 44, 79–89.

Vacchi, M., Rovere, A., Chatzipetros, A., Zouros, N., Firpo, M., 2014. An updated database of Holocene relative sea-level changes in NE Aegean Sea. Quat. Int. 328–329, 301–310.

Vacchi, M., Marriner, N., Morhange, C., Spada, G., Fontana, A., Rovere, A., 2016. Multiproxy assessment of Holocene relative sea-level changes in the western Mediterranean: sea-level variability and improvements in the definition of the isostatic signal. Earth Sci. Rev. 155, 172–197. https://doi.org/10.1016/j.earscirev.2016.02.002.

Vacchi, M., Ghilardi, M., Spada, G., Currás, A., Robresco, S., 2017. New insights into the sea-level evolution in Corsica (NW Mediterranean) since the late Neolithic. J. Archaeol. Sci.: Report. https://doi.org/10.1016/j.jasrep.2016.07.006.

Vacchi, M., Ghilardi, M., Melis, R.T., Spada, G., Giaime, M., Marriner, N., Lorscheid, T., Morhange, C., Burjachs, F., Rovere, A., 2018. New relative sea-level insights into the isostatic history of the western Mediterranean. Quat. Sci. Rev. 201, 396–408. https://doi.org/10.1016/J.QUASCIREV.2018.10.025.

Vamvakaris, D.A., Papazachos, C.B., Papaioannou, C.A., Scordilis, E.M., Karakaisis, G.F., 2016. A detailed seismic zonation model for shallow earthquakes in the broader Aegean area. Nat. Hazards Earth Syst. Sci. 16 (1), 55–84.

Vouvalidis, K., Syrides, G., Pavlopoulos, K., Pechlivanidou, S., Tsourlos, P., Papakonstantinou, M., 2010. Palaeogeographical reconstruction of the battle terrain in Ancient Thermopylae, Greece. Geodin. Acta 23, 241–253.